Nonlinear Dispersion of Surface Gravity Waves in Shallow Water*

T. H. C. HERBERS

Department of Oceanography, Naval Postgraduate School, Monterey, California

STEVE ELGAR

Department of Applied Ocean Physics and Engineering, Woods Hole Oceanographic Institution, Woods Hole, Massachusetts

N. A. SARAP

Department of Oceanography, Naval Postgraduate School, Monterey, California

R. T. GUZA

Center for Coastal Studies, Scripps Institution of Oceanography, La Jolla, California

(Manuscript received 23 May 2000, in final form 27 August 2001)

ABSTRACT

The nonlinear dispersion of random, directionally spread surface gravity waves in shallow water is examined with Boussinesq theory and field observations. A theoretical dispersion relationship giving a directionally averaged wavenumber magnitude as a function of frequency, the local water depth, and the local wave spectrum and bispectrum is derived for waves propagating over a gently sloping beach with straight and parallel depth contours. The linear, nondispersive shallow water relation is recovered as the first-order solution, with weak frequency and amplitude dispersion appearing as second-order corrections. Wavenumbers were estimated using four arrays of pressure sensors deployed in 2–6-m depth on a gently sloping sandy beach. When wave energy is low, the observed wavenumbers agree with the linear, finite-depth dispersion relation over a wide frequency range. In high energy conditions, the observed wavenumbers deviate from the linear dispersion relation by as much as 20%–30% in the frequency range from two to three times the frequency of the primary spectral peak, but agree well with the nonlinear Boussinesq dispersion relation, confirming that the deviations from linear theory are finite amplitude effects. In high energy conditions, the predicted frequency and amplitude dispersion tend to cancel, yielding a nearly nondispersive wave field in which waves of all frequencies travel with approximately the linear shallow water wave speed, consistent with the observations. The nonlinear Boussinesq theory wavenumber predictions (based on the assumption of irrotational wave motion) are accurate even within the surf zone, suggesting that wave breaking on gently sloping beaches has little effect on the dispersion relation.

1. Introduction

Ocean surface gravity waves are affected by nonlinear interactions between triads of wave components with frequencies (ω) and (vector) wavenumbers ($\vec{k}$) satisfying

$$|\omega_1 \pm \omega_2 \pm \omega_3| = \delta\omega, \tag{1a}$$

$$|\vec{k}_1 \pm \vec{k}_2 \pm \vec{k}_3| = \delta\kappa. \tag{1b}$$

The frequencies ω_i and wavenumber magnitudes $\kappa_i = |\vec{k}_i|$ obey the linear dispersion relation for freely propagating waves

$$\omega^2 = g\kappa \tanh(\kappa h), \tag{2}$$

where g is gravity, h is the water depth, and a nonzero value of either $\delta\omega$ or $\delta\kappa$ defines a mismatch from resonance.

Triads are resonant ($\delta\omega = \delta\kappa = 0$) only for unidirectional waves in the shallow water limit $\kappa h \to 0$ (Phillips 1960). In deep ($\kappa h \gg 1$) and intermediate [$\kappa h = O(1)$] water depths triads are nonresonant (i.e., either $\delta\omega \neq 0$ or $\delta\kappa \neq 0$). Two free primary waves ($\omega_1, \vec{k}_1$) and ($\omega_2, \vec{k}_2$) force secondary wave components ($\omega_1 \pm \omega_2, \vec{k}_1 \pm \vec{k}_2$) that do not obey the dispersion relation (2) and remain small in amplitude.

* Woods Hole Oceanographic Institution Contribution Number 10061.

Corresponding author address: Dr. Thomas H. C. Herbers, Department of Oceanography, Code OC/He, Naval Postgraduate School, Monterey, CA 93943-5122.
E-mail: thherber@nps.navy.mil

However, the spectral levels of these ''bound waves'' can exceed free wave spectral levels at high frequencies, and the associated substantial deviations $\delta\kappa$ from the linear dispersion relation (2) are observed readily (e.g., Mitsuyasu et al. 1979; Donelan et al. 1985; Herbers and Guza 1994). Nonlinear shifts in the dispersion relation of free waves result from third-order amplitude dispersion effects (e.g., Longuet-Higgins and Phillips 1962; Willebrand 1975; Masuda et al. 1979; Laing 1986).

In shallow nearshore waters ($\kappa h \ll 1$), where frequency dispersion is weak and the angular spreading of waves arriving from deep water is reduced by refraction, triad interactions are close to resonance (i.e., $|\delta\omega/\omega| \ll 1$, $|\delta\kappa/\kappa| \ll 1$) and the distinct free and secondary-forced waves with much different κ at the same ω that occur in deeper water are no longer present. Near-resonant triad interactions cause strong evolution of wave spectra over distances of only a few wavelengths (Freilich and Guza 1984) and the characteristic steepening and pitching forward of near-breaking wave crests (Elgar and Guza 1985b). These processes are described well by depth-integrated Boussinesq equations for weakly nonlinear, weakly dispersive waves in varying depth (Peregrine 1967). Boussinesq model predictions of the evolution of wave spectra over alongshore uniform beaches are in good agreement with field observations (e.g., Freilich and Guza 1984; Elgar and Guza 1985a; Norheim et al. 1998). Important developments in Boussinesq models include parabolic approximations for depth variations in two dimensions (Liu et al. 1985), matching of the fully dispersive linear solutions in deeper water (e.g., Madsen et al. 1991; Agnon et al. 1993; Kaihatu and Kirby 1995), higher-order approximations (e.g., Dingemans 1997; Madsen and Schäffer 1998; Agnon et al. 1999), fully nonlinear models (Wei et al. 1995), stochastic formulations (e.g., Agnon and Sheremet 1997; Herbers and Burton 1997), and parameterizations of surf zone dissipation (Mase and Kirby 1992; Schäffer et al. 1993; Eldeberky and Battjes 1996). Analyses of field observations indicate that nonlinear triad interactions play a central role in the spectral energy balance in the surf zone (Elgar et al. 1997; Chen et al. 1997; Herbers et al. 2000), as well as farther seaward.

Wave phase speeds observed within and seaward of the surf zone suggest that, in addition to causing spectral energy transfers, nonlinearity affects the dispersion relation (e.g., Thornton et al. 1976; Thornton and Guza 1982; Stive 1984). The theory for the nonlinear dispersion of periodic waves in uniform depth is well established [see Whitham (1974) for a review] and has been used to heuristically correct wave phase speeds in linear refraction models (Dingemans 1997, and references therein). Nonlinear dispersion effects on random waves in shallow water are less well understood. Freilich and Guza (1984) and Elgar and Guza (1985a) compared the observed phase evolution of nonbreaking shoaling waves with linear theory [Eq. (2)] and with a nonlinear Boussinesq model for unidirectional waves. For energetic narrowband swell, large errors were noted in the linear phase predictions at frequencies corresponding to harmonics of the primary swell peak, whereas nonlinear model predictions were accurate. Observed wave phase speeds, estimated from measured phase differences between closely spaced sensors in a cross-shore array, indicated that high-frequency harmonic components in a narrowband wave field travel with the same (or slightly larger) speeds as the dominant swell components, consistent with the Boussinesq model predictions. In contrast, for low-energy, broadband wave fields the linear model was more accurate than the Boussinesq model, possibly because directional effects were neglected in the nonlinear model.

Here, nonlinear effects on the dispersion relation of random waves in shallow water are examined further by including directional spreading in both the Boussinesq theory and in the analysis of extensive new field observations. Additionally, an explicit theoretical dispersion relation is derived that clarifies the relationship between nonlinear dispersion and the wave spectrum and bispectrum.

In the linear approximation the wavenumber magnitude κ of each wave component, defined here as the local gradient $|\nabla S|$ of the phase function S, depends only on the frequency ω and water depth h [Eq. (2)]. Weak nonlinear interactions with other components cause deviations from the linear dispersion relation. There is no unique relation between ω and κ in a directionally spread, nonlinear wave field because two wave components with the same frequency ω that propagate in different directions undergo different interactions, and thus experience a different net nonlinear wavenumber shift. That is, sea surface fluctuations at frequency ω contain a range of wavenumber magnitudes rather than a single κ value. An average wavenumber magnitude at frequency ω, $\kappa_{\text{rms}}(\omega)$, is defined here as a local root-mean-square average of κ over all directional components with frequency ω

$$\kappa_{\text{rms}}(\omega) \equiv \left[\frac{\displaystyle\int_{-\infty}^{\infty}\int_{-\infty}^{\infty} d\vec{k}|\vec{k}|^2 E(\omega, \vec{k})}{\displaystyle\int_{-\infty}^{\infty}\int_{-\infty}^{\infty} d\vec{k} E(\omega, \vec{k})} \right]^{1/2} \tag{3}$$

with $E(\omega, \vec{k})$ the local wavenumber–frequency spectrum. In section 2 an expression for $\kappa_{\text{rms}}(\omega)$ is derived from Boussinesq theory. Accurate estimates of $\kappa_{\text{rms}}(\omega)$, within and seaward of the surf zone, were obtained with four arrays of near-bottom pressure sensors deployed for four months along a cross-shore transect on a gently sloping, sandy beach (section 3). Observed wavenumbers are

compared with the linear dispersion relation (2) and with nonlinear Boussinesq theory predictions for three case studies (including both nonbreaking and breaking waves) in section 4, and for the entire dataset in section 5. Boussinesq wavenumber predictions are generally within 5% of the observations, including high-energy conditions when deviations from the linear dispersion relation (2) are as large as 20%–30%. The results are summarized in section 6.

2. Theory

The sea surface elevation $\eta(x, y, t)$ of surface gravity waves propagating over a beach with straight and parallel depth contours [$h = h(x)$] has the general Fourier representation:

$$\eta(x, y, t) = \sum_{p=-\infty}^{\infty} \sum_{q=-\infty}^{\infty} A_{p,q}(x) \exp[i(l_q y - \omega_p t)], \quad (4)$$

where $\omega_p = p\Delta\omega$ and $l_q = q\Delta l$ are the frequency and alongshore wavenumber (with $\Delta\omega$ and Δl the separation of adjacent bands), x and y are cross-shore and alongshore coordinates, and t is time. The complex function $A_{p,q}$ incorporates the cross-shore variation of both the amplitude and phase of component p, q. Three small parameters, dispersion δ, nonlinearity ε, and medium variations γ, are defined as

$$\delta \equiv \kappa_0 h_0 \ll 1, \quad (5a)$$

$$\varepsilon \equiv a_0/h_0 \ll 1, \quad (5b)$$

$$\gamma \equiv \beta_0/(\kappa_0 h_0) \ll 1, \quad (5c)$$

where κ_0, a_0, h_0, and β_0 are a representative wavenumber, wave amplitude, water depth, and bottom slope, respectively. Using the standard Boussinesq approximation and assuming that appreciable depth variations occur over the same scale as nonlinear energy exchanges,

$$\delta^2 \sim \varepsilon \sim \gamma,$$

the evolution equation for $A_{p,q}$ in dimensional form is [Eq. (11) in Herbers and Burton 1997]

$$\frac{dA_{p,q}}{dx} = \frac{i\omega_p A_{p,q}}{(gh)^{1/2}}\left[1 + \underbrace{\frac{ig^{1/2}}{4\omega_p h^{1/2}}\frac{dh}{dx}}_{(\gamma)} + \underbrace{\frac{h\omega_p^2}{6g}}_{(\delta^2)} - \underbrace{\frac{ghl_q^2}{2\omega_p^2}}_{(\delta^2)} - \underbrace{\frac{3}{4hA_{p,q}}\sum_{m=-\infty}^{\infty}\sum_{n=-\infty}^{\infty} A_{m,n}A_{p-m,q-n}}_{(\varepsilon)}\right]. \quad (6)$$

Imaginary terms inside the brackets yield wave amplitude changes, whereas real terms yield phase changes that define the local cross-shore wavenumber k. The leading-order term gives the fast phase changes of the lowest-order unidirectional, shallow water wave motion with wavenumber $\omega/(gh)^{1/2}$. The remaining terms are slow amplitude and phase changes that are $O(\gamma)$, $O(\delta^2)$, or $O(\varepsilon)$ smaller than the leading term. The second term [$O(\gamma)$] describes amplitude variations associated with linear shoaling (i.e., changes in wave group speed). The third term [$O(\delta^2)$] is a phase correction that describes the increase of k caused by frequency dispersion. The fourth term reduces k for obliquely propagating waves. Owing to refraction the alongshore wavenumber l is $O(\delta)$ smaller than k, yielding a term of the same order [$O(\delta^2)$] as the frequency dispersion term. Nonlinear amplitude and phase changes are given by the last term [$O(\varepsilon)$] in Eq. (6). The underlying assumptions of weak dispersion and alongshore uniformity limit applications of Eqs. (4) and (6) to a narrow shallow water region near the shore (depths less than about 7 m for typical ocean wave conditions) on beaches with alongshore depth variations that are at least $O(\delta)$ smaller than cross-shore variations (nominally $dh/dy \lesssim 0.3\ dh/dx$).

To determine a root-mean-square average wavenumber magnitude $\kappa_{\rm rms}(\omega)$ as a function of frequency [Eq. (3)], sea surface slope statistics are evaluated. The x and y derivatives of Eq. (4) are

$$\eta_x(x, y, t) = \sum_{p=-\infty}^{\infty} \sum_{q=-\infty}^{\infty} \frac{dA_{p,q}(x)}{dx} \exp[i(l_q y - \omega_p t)] \quad (7a)$$

$$\eta_y(x, y, t) = \sum_{p=-\infty}^{\infty} \sum_{q=-\infty}^{\infty} il_q A_{p,q}(x) \exp[i(l_q y - \omega_p t)]. \quad (7b)$$

The frequency–alongshore wavenumber spectra of $\eta_x(E_{p,q}^{\eta_x})$ and $\eta_y(E_{p,q}^{\eta_y})$ are obtained by squaring and time averaging the Fourier transforms of Eqs. (7a) and (7b), substituting Eq. (6) (using the symmetry relations $\omega_{-p} = -\omega_p$, $l_{-q} = -l_q$, and $A_{-p,-q}$ is the complex conjugate of $A_{p,q}$), and retaining terms to orders δ^2, ε, and γ, yielding

$$E_{p,q}^{\eta_x} = \left\langle \frac{dA_{p,q}}{dx}\frac{dA_{-p,-q}}{dx} \right\rangle = \frac{\omega_p^2}{gh}E_{p,q}\left(1 + \underbrace{\frac{\omega_p^2 h}{3g}}_{(\delta^2)} - \underbrace{\frac{ghl_q^2}{\omega_p^2}}_{(\delta^2)} - \underbrace{\frac{3}{2hE_{p,q}}\sum_{m=-\infty}^{\infty}\sum_{n=-\infty}^{\infty} \mathrm{Re}\{B_{m,n,p-m,q-n}\}}_{(\varepsilon)} + O(\delta^4, \delta^2\varepsilon, \varepsilon^2, \varepsilon\gamma, \gamma^2)\right) \quad (8a)$$

$$E_{p,q}^{\eta_y} = \langle il_q A_{p,q} il_{-q} A_{-p,-q} \rangle = l_q^2 E_{p,q}, \quad (8b)$$

where angle brackets indicate the expected value, Re{ } denotes the real part, and the spectrum E and bispectrum B describe the second-, and third-order statistics of the sea surface elevation amplitudes:

$$E_{p,q} \equiv \langle A_{p,q} A_{-p,-q} \rangle, \tag{9a}$$

$$B_{m,n,p-m,q-n} \equiv \langle A_{m,n} A_{p-m,q-n} A_{-p,-q} \rangle. \tag{9b}$$

Bottom slope effects do not appear in Eq. (8a) because the linear shoaling gradient of $A_{p,q}$ [the $O(\gamma)$ term in Eq. (6)] is in quadrature with the $O(1)$ phase variation of $A_{p,q}$. Amplitude variations resulting from both linear shoaling and nonlinear interactions [the imaginary part of the $O(\varepsilon)$ term in Eq. (6)] contribute to Eq. (8a) at higher order (ε^2, $\varepsilon\gamma$, and γ^2), and are neglected here.

To the present order, all terms retained in the slope spectrum $E^{\eta_x}_{p,q}$ represent phase variations, and thus a local root-mean-square average value of the cross-shore wavenumber $k_{p,q}$ of waves with frequency ω_p and alongshore wavenumber l_q can be obtained by substituting $E^{\eta_x}_{p,q} = k^2_{p,q} E_{p,q}$ into the left-hand side of Eq. (8a).

In the limit of infinitesimal separation between adjacent spectral components, a continuous density spectrum

$$E_{p,q} \equiv E(\omega_p, l_q) \Delta\omega \Delta l$$

and bispectrum

$$B_{m,n,p-m,q-n} \equiv B(\omega_m, l_n, \omega_{p-m}, l_{q-n})(\Delta\omega)^2(\Delta l)^2$$

can be defined, and the slope spectra [Eqs. (8a,b)] are

$$E^{\eta_x}(\omega, l) = \left(\frac{\omega^2}{gh} + \frac{\omega^4}{3g^2} - l^2\right) E(\omega, l) - \frac{3\omega^2}{2gh^2} \int_{-\infty}^{\infty} \int_{-\infty}^{\infty} d\omega'\, dl' \,\mathrm{Re}\{B(\omega', l', \omega - \omega', l - l')\} \tag{10a}$$

$$E^{\eta_y}(\omega, l) = l^2 E(\omega, l). \tag{10b}$$

The root-mean-square average wavenumber $\kappa_{\mathrm{rms}}(\omega)$ of spectral components with frequency ω (Eq. 3) can be expressed in terms of the slope spectra as

$$\kappa_{\mathrm{rms}}(\omega) = \left[\frac{\displaystyle\int_{-\infty}^{\infty} dl [E^{\eta_x}(\omega, l) + E^{\eta_y}(\omega, l)]}{\displaystyle\int_{-\infty}^{\infty} dl E(\omega, l)} \right]^{1/2}. \tag{11}$$

Substitution of Eqs. (10a,b) in Eq. (11) yields the dispersion relation:

$$\kappa_{\mathrm{rms}}(\omega) = \kappa_{\mathrm{sw}}(\omega)[1 + \beta_{\mathrm{fr}}(\omega) - \beta_{\mathrm{am}}(\omega)]^{1/2}, \tag{12}$$

where the leading order term $\kappa_{\mathrm{sw}}(\omega)$ is the linear shallow water dispersion relation

$$\kappa_{\mathrm{sw}}(\omega) = \frac{\omega}{(gh)^{1/2}}, \tag{13}$$

and $\beta_{\mathrm{fr}}(\omega)$ and $\beta_{\mathrm{am}}(\omega)$ describe second-order frequency and amplitude dispersion effects, respectively:

$$\beta_{\mathrm{fr}}(\omega) = \frac{h\omega^2}{3g}, \tag{14a}$$

$$\beta_{\mathrm{am}}(\omega) = \frac{3}{2hE(\omega)} \int_{-\infty}^{\infty} d\omega' \,\mathrm{Re}\{B(\omega', \omega - \omega')\} \tag{14b}$$

with $E(\omega)$ and $B(\omega_1, \omega_2)$ the frequency spectrum and bispectrum of η. The amplitude dispersion term $\beta_{\mathrm{am}}(\omega)$ depends inversely on the energy level at frequency ω and is proportional to the real part of the bispectrum integrated over all triads involving frequency ω. For a single $(\omega_1, \omega_2, \omega_3)$ triad, the nonlinear interaction changes the wavenumbers of all three components, and the least energetic component has the largest relative change [Eq. (14b); see also Freilich and Guza (1984)]. Although Eqs. (12)–(14) do not depend explicitly on the wave directional properties or the bathymetry $h(x)$, the shoaling evolution of the spectrum $E(\omega)$ and bispectrum $B(\omega_1, \omega_2)$ depends on these parameters. Locally measured values of $E(\omega)$ and $B(\omega_1, \omega_2)$ are used here to evaluate β_{am}.

The theoretical dispersion relationship for random, weakly nonlinear, and directionally spread waves in shallow water [Eqs. (12)–(14)] is verified with field measurements described next.

3. Field experiment and analysis

Detailed measurements of shoaling waves on an ocean beach were collected at the U.S. Army Corps of Engineer's Field Research Facility located near Duck, North Carolina (Elgar et al. 2001). The present study uses data from four arrays, each consisting of six bottom-mounted pressure sensors in a compact two-dimensional configuration with sensor spacings between 4 and 12 m (Fig. 1). The arrays, denoted 4, 5, 6, and 7, were located along a cross-shore transect about 100, 150, 300, and 400 m from the shoreline, in nominal depths of 2.5, 3.5, 4.0, and 5.5 m, respectively. Data were collected nearly continuously with a sample frequency of 2 Hz from 2 August through 4 December 1997. Array 4 did not operate from 17 to 29 October and from 2 to 11 November. Array 6 did not operate from 14 November through the end of the experiment. Mean horizontal currents were measured with electro-

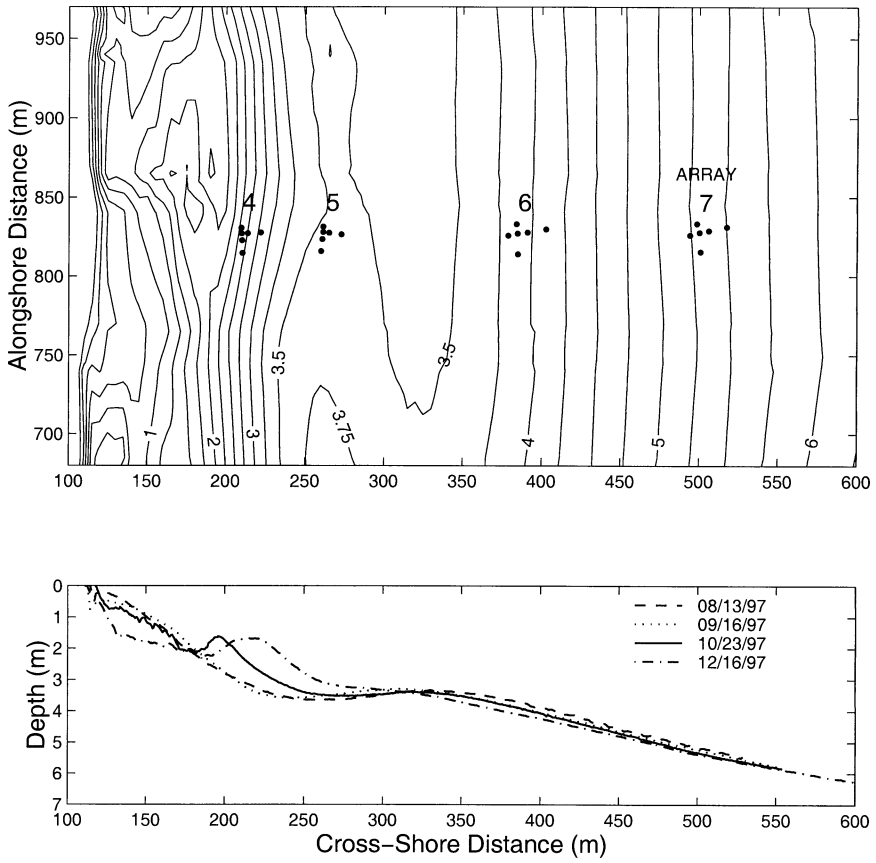

FIG. 1. (a) Plan view of the four arrays (numbered 4–7), each consisting of six bottom-mounted pressure sensors (filled circles). Locations are given in the local beach coordinate system of the Field Research Facility. Solid curves indicate depth contours in m (relative to mean sea level), based on a survey conducted on 23 Oct 1997. (b) Beach profiles along the instrumented transect obtained from four surveys that span the duration of the experiment.

magnetic current meters at each array. Measurements of the offshore incident wave field were acquired with a directional wave buoy in 20-m depth, 5 km from shore. Local winds were measured with anemometers mounted on a nearby pier.

The bathymetry in the instrumented region was gently sloping (<0.02) in the cross-shore direction and approximately uniform in the alongshore direction (Fig. 1). A shore-parallel sand bar remained relatively stationary between arrays 6 and 5 with its crest submerged about 3.5 m below sea level. The bathymetry inshore of array 5 was more dynamic, with a transient shore-parallel bar near array 4 that was submerged about 1.5–2 m below sea level.

A root-mean-square average wavenumber as a function of frequency, $\kappa_{\rm rms}(\omega)$ (Eq. 3), was estimated with an existing method (Herbers and Guza 1994; Herbers et al. 1995). The array aperture D is assumed small compared with the scales of depth variations and nonlinear energy exchanges ($\kappa D \ll \gamma^{-1}, \varepsilon^{-1}$) so that the wave field over the array can be approximated as spatially homogeneous:

$$\eta(\vec{x}, t) = \int_{-\infty}^{\infty}\int_{-\infty}^{\infty}\int_{-\infty}^{\infty} dZ(\omega, \vec{k}) \exp[i(\vec{k}\cdot\vec{x} - \omega t)], \quad (15)$$

where $dZ(\omega, \vec{k})$ is a Fourier–Stieltjes amplitude. The cross-spectrum $H_{ij}(\omega)$ of a pair of sensors at locations $\vec{x}_i$ and $\vec{x}_j$ is given by

$$H_{ij}(\omega) = \int_{-\infty}^{\infty}\int_{-\infty}^{\infty} d\vec{k} \exp[i\vec{k}\cdot(\vec{x}_i - \vec{x}_j)]E(\omega, \vec{k}), \quad (16)$$

where $E(\omega, \vec{k})$ is the wavenumber–frequency spectral density

$$E(\omega, \vec{k})d\omega d\vec{k} \equiv \langle |dZ(\omega, \vec{k})|^2 \rangle. \quad (17)$$

The wavenumber $\kappa_{\rm rms}(\omega)$ was estimated with a linear sum of the normalized cross-spectra

$$\kappa_{\rm rms}(\omega) = \left[\sum_{i=1}^{N}\sum_{j=1}^{N} \alpha_{ij}\frac{H_{ij}(\omega)}{\sqrt{H_{ii}(\omega)H_{jj}(\omega)}}\right]^{1/2}, \quad (18)$$

where N is the number of array sensors and α_{ij} are weighting coefficients. Substitution of Eq. (16) in Eq. (18) yields

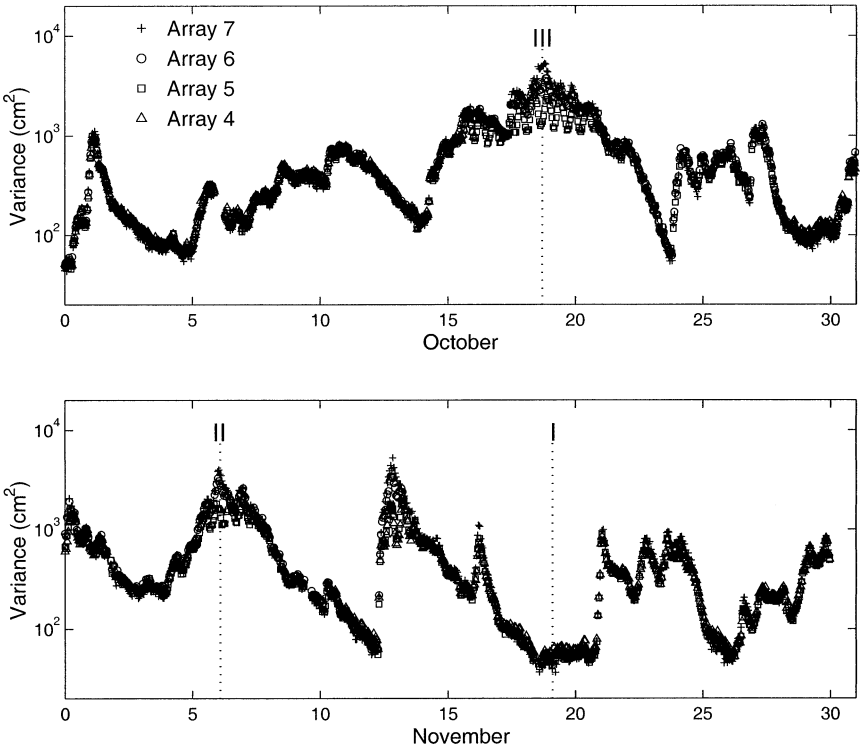

FIG. 2. Wave variance observed at the four arrays vs time during Oct and Nov 1997. The variance estimates were obtained by transforming the measured pressure spectra to surface elevation spectra with linear finite depth theory, and then integrating over the swell–sea frequency range, 0.05–0.25 Hz. Three case studies analyzed in Figs. 3–5 are indicated with vertical dotted lines labeled I–III.

$$\kappa_{\text{rms}}(\omega) = \left[\frac{\int_{-\infty}^{\infty} \int_{-\infty}^{\infty} d\vec{k} F(\vec{k}) E(\omega, \vec{k})}{\int_{-\infty}^{\infty} \int_{-\infty}^{\infty} d\vec{k} E(\omega, \vec{k})} \right]^{1/2} \tag{19}$$

with the kernel function $F(\vec{k})$ given by

$$F(\vec{k}) = \sum_{i=1}^{N} \sum_{j=1}^{N} \alpha_{ij} \exp[i\vec{k} \cdot (\vec{x}_i - \vec{x}_j)]. \tag{20}$$

Optimal coefficients α_{ij} were determined a priori through a least squares fit of the function $F(\vec{k})$ to $|\vec{k}|^2$ [cf. Eqs. (19) and (3)] using an expansion of the exponential terms in Eq. (20) for small $\vec{k} \cdot (\vec{x}_i - \vec{x}_j)$ [see Herbers et al. (1995) for details]. The wavenumber estimates are restricted to the frequency range (0.05–0.25 Hz) of the dominant swell and sea waves, corresponding to wavelengths (20–130 m) that are resolved well by the arrays and are more than four times the water depth. The frequency resolution of 0.01 Hz ensures statistically stable estimates (approximately 70 degrees of freedom for the 1-h-long data records), while still resolving the main spectral features.

Nonlinear theory-based estimates of $\kappa_{\text{rms}}(\omega)$ were obtained by substituting local observations of h, $E(\omega)$, and $B(\omega_1, \omega_2)$ in Eqs. (12)–(14). The $E(\omega)$ and $B(\omega_1, \omega_2)$ estimates (averaged over the six sensors of the array to enhance statistical stability) assume a hydrostatic pressure-surface elevation transfer function. The neglected second-order terms in this transfer function that account for the weak vertical decay of pressure [e.g., Eq. (A6b) in Herbers and Burton 1997] obey the shallow water dispersion relation [Eq. (13)] of the lowest-order wave motion, and thus do not affect $\kappa_{\text{rms}}(\omega)$ to the present order. The nonlinear interaction integral [Eq. (14b)] was evaluated for the frequency range

$$-\omega_{\max} < \omega', \omega - \omega', \omega < \omega_{\max}$$

with a cutoff frequency $\omega_{\max}/2\pi = 0.5$ Hz that includes the energy-containing part of the wave spectrum.

4. Observed and predicted dispersion relations: Case examples

Nonlinear effects on the dispersion relation of shallow water waves are illustrated here with three case studies selected from a wide range of conditions encountered during the four-month-long experiment (Fig. 2). Cases II and III were collected during storms when the offshore significant wave height $H_s(\equiv 4\sqrt{\langle \eta^2 \rangle})$ exceeded 2 m and several of the arrays were within the surf zone. The nonlinearity parameter ε [estimated as a_{rms}/h with

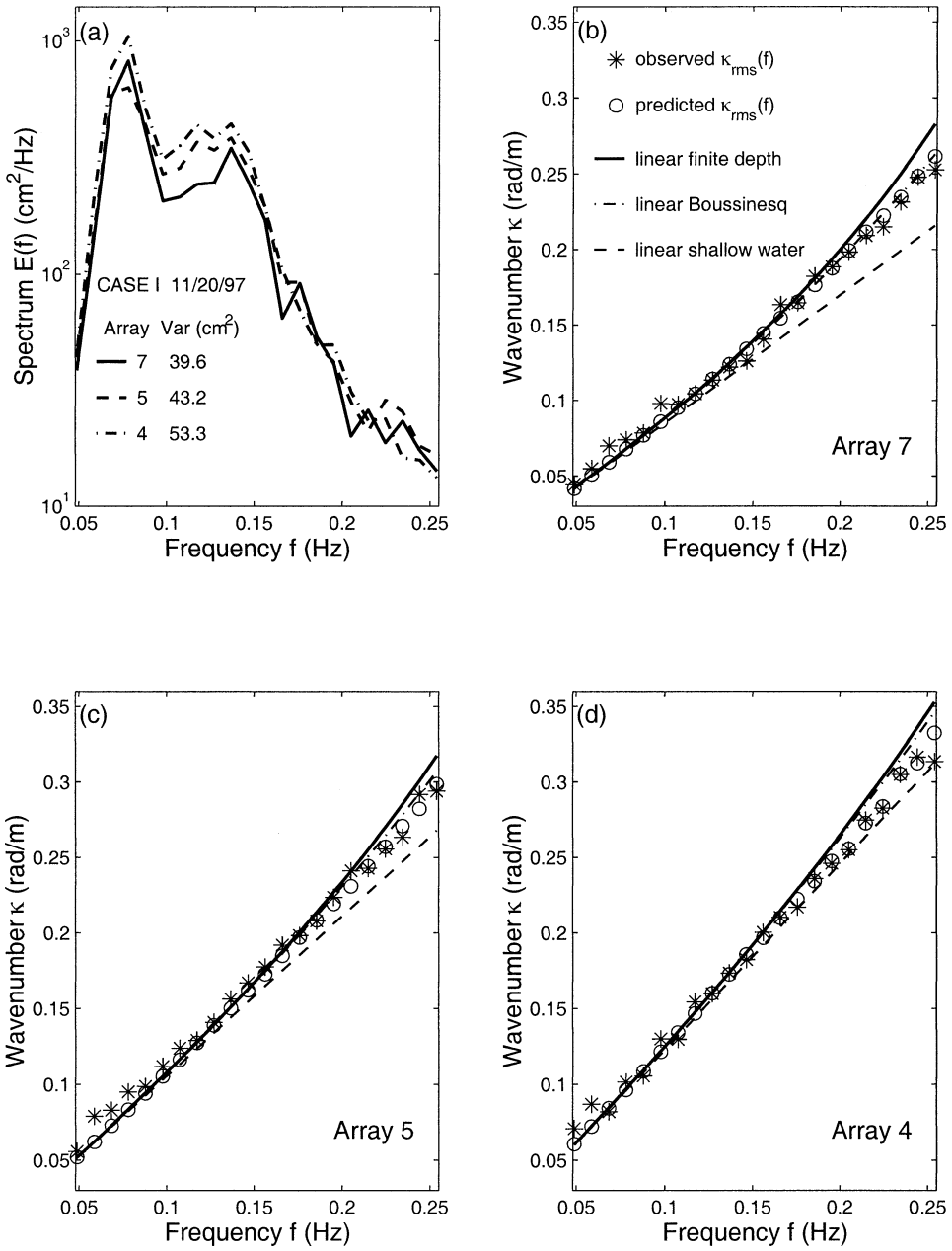

FIG. 3. Comparison of observed with predicted wavenumbers for case I (0200–0300 EST 20 Nov). (a) Observed surface elevation spectra $E(f)$ at each array (estimated from the pressure measurements using linear finite depth theory). The corresponding variances (in the range 0.05–0.25 Hz) are listed. (b–d) For each array, the observed root-mean-square average wavenumber, as a function of frequency, $\kappa_{\rm rms}(f)$ (asterisks) is compared with the dispersion relation of linear finite depth theory [solid curve, Eq. (2)] and with a prediction based on nonlinear Boussinesq theory [circles, Eqs. (12)–(14)]. Also included are the linear shallow water dispersion relation (dashed curve) and the linearized Boussinesq dispersion relation (dash–dot curve).

the root-mean-square amplitude $a_{\rm rms}$ given by the narrowband approximation $a_{\rm rms} \equiv \sqrt{2\langle\eta^2\rangle}$] in these cases ranged between about 0.13 and 0.17. These cases with pronounced nonlinear effects on the dispersion relation are contrasted with case I collected during calm conditions (offshore H_s = 0.3 m) with weak nonlinearity (ε about 0.016–0.038). The observed wave spectrum $E(f)$ (single-sided with $f \equiv \omega/2\pi$) at each array and corresponding wavenumber estimates $\kappa_{\rm rms}(f)$ are shown for the three cases in Figs. 3–5 (in each case, one nonoperating array was excluded from the comparisons).

The observed $\kappa_{\rm rms}(f)$ [Eq. (18)] are compared with

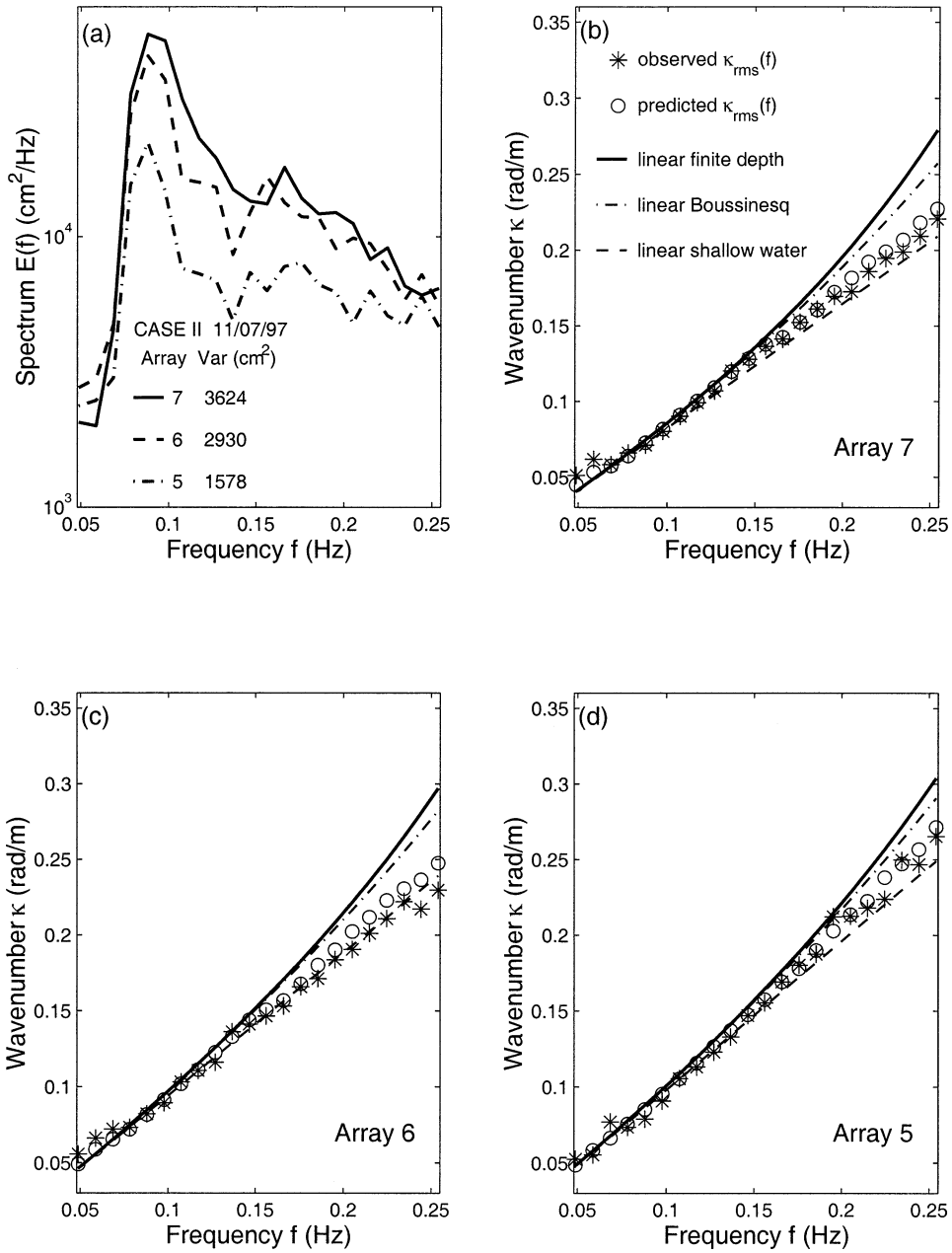

FIG. 4. Comparison of observed with predicted wavenumbers for case II (0200–0300 EST 7 Nov). The format is the same as in Fig. 3.

both the linear finite depth dispersion relation [Eq. (2)] and the nonlinear Boussinesq dispersion relation [Eq. (12)]. To isolate the contributions of frequency dispersion β_{fr} [Eq. (14a)] and amplitude dispersion β_{am} [Eq. (14b)], the linear shallow water dispersion relation $\kappa_{sw}(f)$ [Eq. (13), neglecting both β_{fr} and β_{am}] and the linearized Boussinesq dispersion relation [Eq. (12) excluding β_{am}] also are included in Figs. 3–5. Differences between the linear finite depth and linearized Boussinesq dispersion relations, that result from neglecting $O(\delta^4)$ dispersion terms in the Boussinesq theory, are small. The maximum dispersion error is about 7% at the deepest array (7) and highest frequency (0.25 Hz) included in the present comparisons.

a. Case I. 20 November

Low-energy swell with a peak frequency of 0.07 Hz (Fig. 3a), an offshore significant wave height of 0.3 m, and a mean direction within 15° of normal incidence, was observed in light wind conditions (speeds <5 m s^{-1}). The surf zone was well inshore of the shallowest

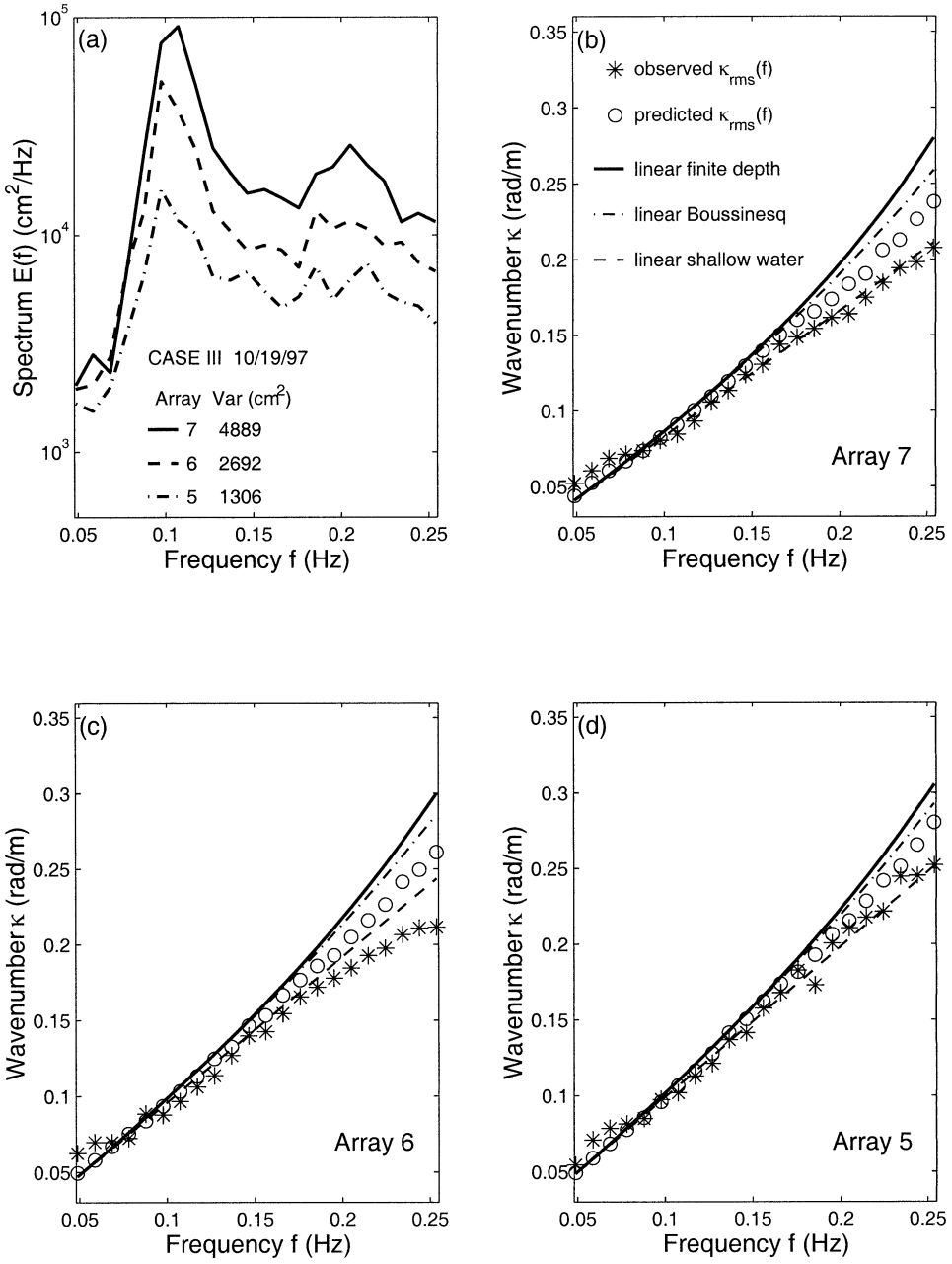

FIG. 5. Comparison of observed with predicted wavenumbers for case III (1600–1700 EST 19 Oct). The format is the same as in Fig. 3.

array and mean currents were weak (<0.05 m s^{-1}). The small increases in variance observed between arrays 7 and 5 (9%) and between arrays 5 and 4 (19%) are consistent with linear shoaling (i.e., the $\propto h^{1/2}$ decrease in group speed in shallow water). Observed wavenumbers agree well with the linear finite depth dispersion relation, and also with nonlinear and linear Boussinesq dispersion relations (Figs. 3b–d), confirming the expected linearity of the wave motion in benign conditions. Amplitude dispersion is weak, but detectable at the highest frequencies, where the nonlinear Boussinesq theory predictions (and the observations) deviate slightly (5%) from the linear dispersion relation.

The predicted $\kappa_{\text{rms}}(f)$ vary smoothly with frequency, but the observed $\kappa_{\text{rms}}(f)$ show some scatter at frequencies below about 0.1 Hz. Previous observations at the same field site show that wave reflection from shore is significant at swell frequencies in low energy conditions (Elgar et al. 1994). The resulting partial standing wave patterns likely contribute significant errors to $\kappa_{\text{rms}}(f)$ estimates based on the assumption of a progressive wave field (e.g., Elgar and Guza 1985a).

b. Case II. 7 November

Swell with a peak frequency $f_p = 0.08$ Hz, offshore significant wave height $H_s = 2.3$ m, and mean direction close to normal incidence was observed when local wind speeds were less than 10 m s^{-1}, indicating that the waves arrived from a remote source. Wave breaking was minimal between the 20-m depth buoy and the deepest array 7, but significant breaking-induced dissipation between the arrays is evident in the observed decrease in swell variance between arrays 7 and 6 (17%) and between arrays 6 and 5 (43%). Mean currents at the arrays were less than about 0.3 m s^{-1}, much smaller than the wave phase speeds (about 5–7 m s^{-1}). At all three arrays the observed $\kappa_{\text{rms}}(f)$ diverge from the linear finite depth dispersion relation at frequencies higher than about $2f_p$. At the highest frequency considered (0.25 Hz, approximately $3f_p$) the observed $\kappa_{\text{rms}}(f)$ are about 25% below the linear dispersion relation (Figs. 4b–d). Nonlinear Boussinesq theory predictions are in excellent agreement with the observed wavenumbers over the entire frequency range. The observed and predicted wavenumbers are close to the shallow water dispersion relation, indicating that the frequency (β_{fr}) and amplitude (β_{am}) dispersion terms in Eq. (12) approximately cancel, yielding a nondispersive wave field in which all components travel with the shallow water wave speed $\sqrt{gh}$.

c. Case III. 19 October

The most energetic waves were observed during the passage of a nor'easter storm with local wind speeds up to 18 m s^{-1}. The offshore significant wave height was about 3.6 m, with a mean direction within 10° of normal incidence. The observed swell variances decreased by 32% between the offshore buoy and array 7, 45% between arrays 7 and 6, and 50% between arrays 6 and 5 (Fig. 5a), indicating that all arrays were located within the surf zone. Similar to case II, the observed $\kappa_{\text{rms}}(f)$ are in good agreement with the linear finite depth dispersion relation at the spectral peak frequency (0.1 Hz), but increasingly diverge from linear theory at higher frequencies, with discrepancies as large as 30% at the deeper arrays 6 and 7 (Figs. 5b,c). The nonlinear Boussinesq theory predictions are (as in case II) close to the shallow water dispersion relation, indicating canceling frequency and amplitude dispersion effects. The agreement between nonlinear Boussinesq theory predictions and observed wavenumbers is not as good as in case II (cf. Fig. 4 with Fig. 5), and observed wavenumbers are about 5%–15% smaller than predicted at high frequencies. Mean currents were strong in case III (up to 1.35 m s^{-1}), but nearly perpendicular to the dominant wave directions at all frequencies, and thus Doppler shifts were small. The cause of the increased errors in case III is unknown, but neglected higher-order nonlinear effects and wave breaking may be a significant source of errors in this most energetic case.

5. Accuracy of predicted dispersion relations

The limited validity of the linear finite depth dispersion relation (2) and the improved accuracy of the weakly nonlinear Boussinesq dispersion relation (12)–(14) are demonstrated here for the entire dataset. To relate the accuracy of dispersion relations to wave energy levels, the data for each array were binned into 10 equal log-spaced classes of local wave variance. For each class the mean and standard deviation of the ratio between predicted and observed $\kappa_{\text{rms}}(f)$ were computed at the peak (f_p) and harmonic ($2f_p$, $3f_p$) frequencies (Fig. 6).

At the peak frequency f_p (Figs. 6a,b), both linear and nonlinear theory predictions agree well with observations. At the maximum variance levels the linear dispersion relation overpredicts the observed wavenumbers by about 5%, whereas the nonlinear wavenumber predictions are slightly more accurate, indicating that nonlinearity causes a small decrease in wavenumber (i.e., increase in wave speed). Standard deviations of predicted/observed wavenumbers (not shown) are similar for the linear and nonlinear models and range from 0.16 at array 4 in low energy conditions to less than 0.01 at array 7 in high energy conditions. As discussed above, scatter in observed wavenumbers may result from partial standing wave patterns that are most pronounced for small amplitude waves close to shore. These results indicate that nonlinear effects on the dispersion relation are weak at the spectral peak frequency.

Nonlinear effects on the dispersion relation are more evident in the systematic large discrepancies (up to 30%) between observed wavenumbers and linear theory predictions at the harmonic frequencies $2f_p$ and $3f_p$ (Figs. 6c–f). At all arrays, the linear wavenumber is consistently larger than the observed wavenumber, and this bias (i.e., the deviation of the predicted/observed ratio from 1) increases with both increasing frequency and increasing wave variance. The nonlinear wavenumber predictions have small bias (less than a few percent, Figs. 6c–f) and low scatter (standard deviations less than 1%, not shown).

To summarize the overall agreement of observed and predicted wavenumbers, the observed bulk (i.e., frequency-integrated) average wavenumber κ_{rms}

$$\kappa_{\text{rms}} \equiv \left[\frac{\int_{0.05\,\text{Hz}}^{0.25\,\text{Hz}} df\, \kappa_{\text{rms}}^2(f) E(f)}{\int_{0.05\,\text{Hz}}^{0.25\,\text{Hz}} df E(f)} \right]^{1/2} \tag{21}$$

is compared with predictions of κ_{rms} based on linear finite depth and nonlinear Boussinesq theories (Fig. 7). At each array the linear wavenumber predictions have a positive bias that is less than 5% in low energy con-

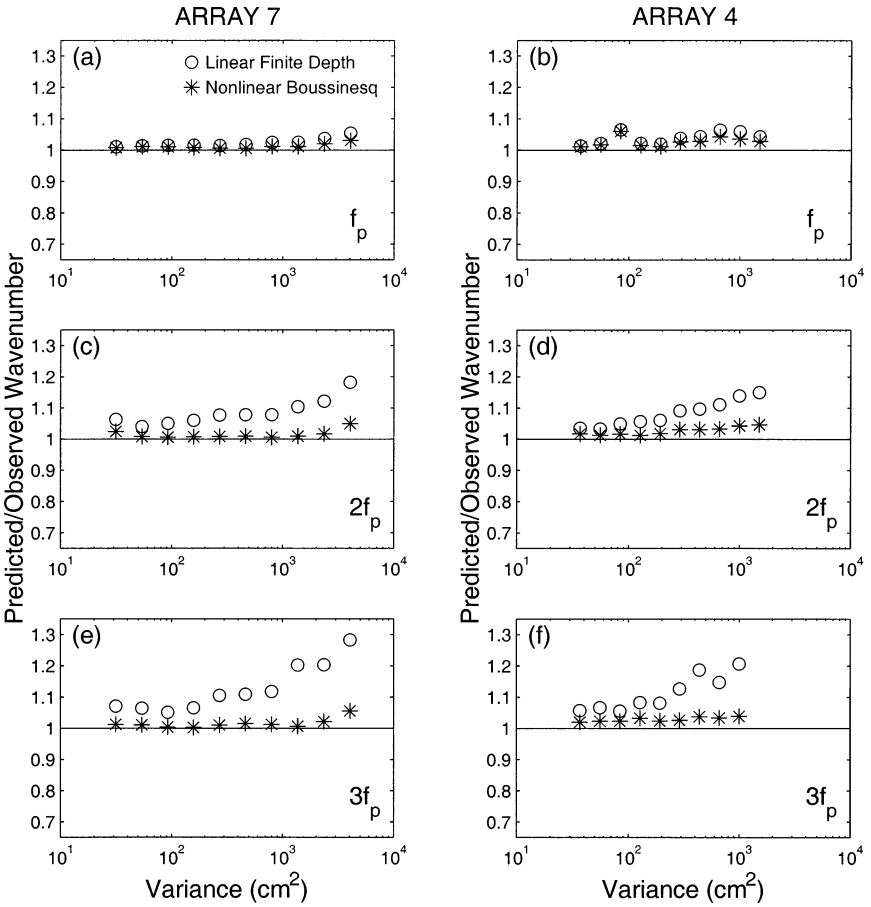

FIG. 6. Ratio of predicted to observed wavenumber vs local wave variance. The data are binned in 10 equal log-spaced classes of total (0.05–0.25 Hz) wave variance that contain between 24 and 527 data records. For each variance bin the mean value of the ratio of the linear finite depth theory prediction [Eq. (2)] to the observed wavenumber is indicated with a circle, and the mean value of the ratio of the nonlinear Boussinesq theory prediction [Eq. (12)–(14)] to the observed wavenumber is indicated with an asterisk. Results for arrays 7 (left) and 4 (right) are given at frequencies: (a–b) f_p (excluding cases with $f_p > 0.25$ Hz), (c–d) $2f_p$ (excluding cases with $2f_p > 0.25$ Hz), and (e–f) $3f_p$ (excluding cases with $3f_p > 0.25$ Hz). Results for the other two arrays (not shown) are similar.

ditions and increases to about 10%–15% in high energy conditions. The bias is largest at the deeper arrays 6 and 7 for reasons that are not understood. The nonlinear wavenumber predictions generally are within a few percent of the observed wavenumbers in low to moderate energy conditions. The approximately 5% overprediction at the highest energy levels may be owing to higher-order nonlinearity or to wave breaking.

6. Summary

Nonlinear effects on the dispersion relation of surface gravity waves in shallow water predicted by weakly nonlinear, weakly dispersive Boussinesq theory agree well with extensive field observations. A theoretical analysis of directionally spread waves propagating over a gently sloping seabed with straight and parallel depth contours yields a nonlinear dispersion relation between a root-mean-square average wavenumber $\kappa_{\rm rms}$ [Eq. (3)] and the wave frequency ω that depends on the local water depth, wave spectrum, and bispectrum [Eqs. (12)–(14)]. The linear shallow water dispersion relation is recovered as the first-order solution, with second-order correction terms for the (usually competing) effects of frequency dispersion (e.g., wave speed decreases with increasing frequency) and amplitude dispersion (e.g., wave speed increases with increasing amplitude).

Four arrays of pressure sensors were deployed between 2 and 6-m depth on a gently sloping ocean beach (Fig. 1) during a four-month period that spanned a wide range of conditions (Fig. 2). Estimates of $\kappa_{\rm rms}(\omega)$ from 1-h-long array records were compared with the linear finite depth dispersion relation and with nonlinear Boussinesq theory predictions. In low energy conditions the observed wavenumbers are close to both the linear and nonlinear dispersion relations, consistent with the pre-

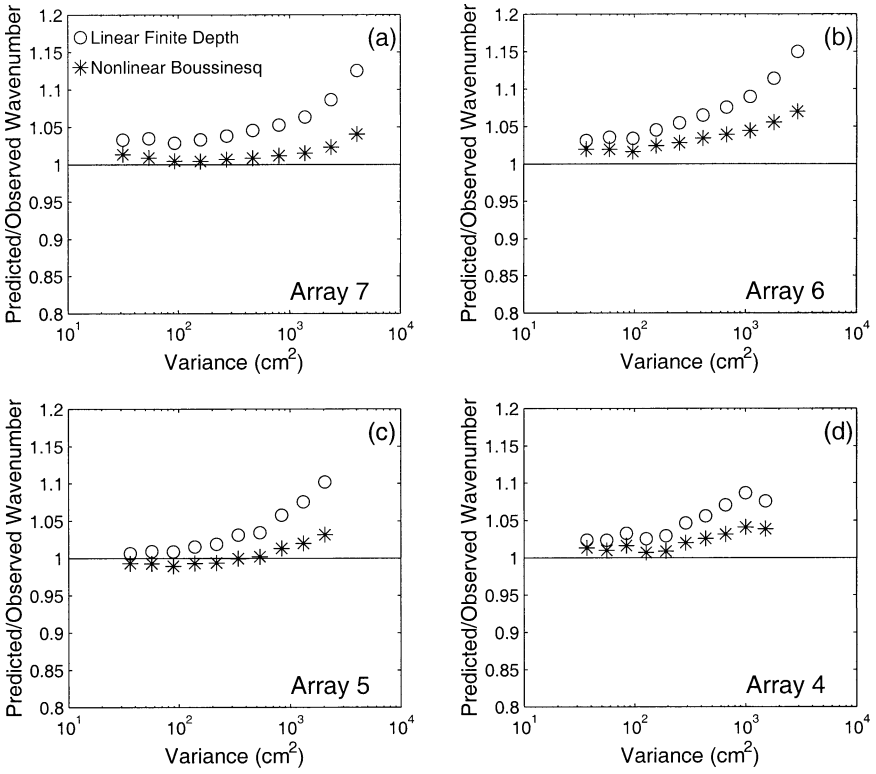

FIG. 7. Ratio of predicted to observed bulk average wavenumber κ_{rms} [Eq. (21)] vs total wave variance for all four arrays. No data are excluded. The format is similar to Fig. 6.

dicted weak amplitude dispersion (Fig. 3). In high energy conditions the observed wavenumbers deviate significantly from the linear dispersion relation, and generally agree well with the nonlinear dispersion relation (Figs. 4, 5). The predicted effects of frequency and amplitude dispersion tend to cancel, so that all components of the wave spectrum travel with approximately the linear shallow water wave speed, consistent with the observations. Wave breaking, not included in the theoretical predictions of $\kappa_{rms}(\omega)$, does not appear to distort substantially the dispersion relation on this gently sloping beach.

Analysis of the entire dataset shows that deviations from the linear finite depth dispersion relation increase systematically with increasing total wave energy (Fig. 7), with discrepancies as large as 20%–30% at frequencies between two and three times the spectral peak frequency (Fig. 6). At all wave energy levels and frequencies, the nonlinear Boussinesq theory predictions are within 2%–7% of the observed wavenumbers.

The dispersion relation presented here [Eq. (12)] clarifies and quantifies the effect of nonlinearity on the wavenumbers of random waves in shallow water. This simple spectral relation potentially is useful for evaluating the local wavenumber properties in stochastic wave shoaling models, and may improve methods for interpreting in situ and remote sensing observations of waves in shallow water that rely on the linear dispersion relation.

Acknowledgments. This research was supported by the Coastal Dynamics Program of the Office of Naval Research and the National Oceanographic Partnership Program (NOPP). We thank the staff of the Scripps Institution of Oceanography Center for Coastal Studies, including Bill Boyd, Kimball Millikan, Brian Woodward, Dennis Darnell, Kent Smith, and Yul Elgar for their tireless and heroic efforts to maintain a large array of instruments on an exposed ocean beach for four months. We also thank Britt Raubenheimer for her contributions to the field data collection and Paul Jessen for assistance in the data analysis. Excellent logistical support, bathymetry and instrument location surveys, and environmental data were provided generously by the Field Research Facility of the U.S. Army Engineer Waterways Experiment Station's Coastal Engineering Research Center. Permission to use these data is appreciated. Reviewers made helpful suggestions.

REFERENCES

Agnon, Y., and A. Sheremet, 1997: Stochastic nonlinear shoaling of directional spectra. *J. Fluid Mech.*, **345,** 79–99.
——, ——, J. Gonsalves, and M. Stiassnie, 1993: Nonlinear evolution

of a unidirectional shoaling wave field. *Coastal Eng.,* **20,** 29–58.
——, P. A. Madsen, and H. A. Schäffer, 1999: A new approach to high-order Boussinesq models. *J. Fluid Mech.,* **399,** 319–333.
Chen, Y., R. T. Guza, and S. Elgar, 1997: Modeling spectra of breaking surface waves in shallow water. *J. Geophys. Res.,* **102,** 25 035–25 046.
Dingemans, M. W., 1997: *Water Wave Propagation over Uneven Bottoms.* Advanced Series on Ocean Engineering, Vol. 13, World Scientific, 967 pp.
Donelan, M. A., J. Hamilton, and W. H. Hui, 1985: Directional spectra of wind-generated waves. *Philos. Trans. Roy. Soc. London,* **A315,** 509–562.
Eldeberky, Y., and J. A. Battjes, 1996: Spectral modeling of wave breaking: Application to Boussinesq equations. *J. Geophys. Res.,* **101,** 1253–1264.
Elgar, S., and R. T. Guza, 1985a: Shoaling gravity waves: Comparisons between field observations, linear theory, and a nonlinear model. *J. Fluid Mech.,* **158,** 47–70.
——, and ——, 1985b: Observations of bispectra of shoaling surface gravity waves. *J. Fluid Mech.,* **161,** 425–448.
——, T. H. C. Herbers, and R. T. Guza, 1994: Reflection of ocean surface gravity waves from a natural beach. *J. Phys. Oceanogr.,* **24,** 1503–1511.
——, R. T. Guza, B. Raubenheimer, T. H. C. Herbers, and E. L. Gallagher, 1997: Spectral evolution of shoaling and breaking waves on a barred beach. *J. Geophys. Res.,* **102,** 15 797–15 805.
——, ——, W. C. O'Reilly, B. Raubenheimer, and T. H. C. Herbers, 2001: Wave energy and direction observed near a pier. *J. Waterway, Port, Coastal, Ocean Eng.,* **127,** 2–6.
Freilich, M. H., and R. T. Guza, 1984: Nonlinear effects on shoaling surface gravity waves. *Philos. Trans. Roy. Soc. London,* **A311,** 1–41.
Herbers, T. H. C., and R. T. Guza, 1994: Nonlinear wave interactions and high-frequency seafloor pressure. *J. Geophys. Res.,* **99,** 10 035–10 048.
——, and M. C. Burton, 1997: Nonlinear shoaling of directionally spread waves on a beach. *J. Geophys. Res.,* **102,** 21 101–21 114.
——, S. Elgar, and R. T. Guza, 1995: Generation and propagation of infragravity waves. *J. Geophys. Res.,* **100,** 24 863–24 872.
——, N. R. Russnogle, and S. Elgar, 2000: Spectral energy balance of breaking waves within the surf zone. *J. Phys. Oceanogr.,* **30,** 2723–2737.
Kaihatu, J. M., and J. T. Kirby, 1995: Nonlinear transformation of waves in finite water depth. *Phys. Fluids,* **7,** 1903–1914.
Laing, A. K., 1986: Nonlinear properties of random gravity waves in water of finite depth. *J. Phys. Oceanogr.,* **16,** 2013–2030.
Liu, P. L.-F., S. B. Yoon, and J. T. Kirby, 1985: Nonlinear refraction-diffraction of waves in shallow water. *J. Fluid Mech.,* **153,** 185–201.
Longuet-Higgins, M. S., and O. M. Phillips, 1962: Phase velocity effects in tertiary wave interactions. *J. Fluid Mech.,* **12,** 333–336.
Madsen, P. A., and H. A. Schäffer, 1998: Higher-order Boussinesq-type equations for surface gravity waves: Derivation and analysis. *Philos. Trans. Roy. Soc. London,* **A356,** 3123–3184.
——, R. Murray, and O. R. Sørensen, 1991: A new form of the Boussinesq equations with improved linear dispersion characteristics. *Coastal Eng.,* **15,** 371–388.
Mase, H., and J. T. Kirby, 1992: Hybrid frequency-domain KdV equation for random wave transformation. *Proc. 23rd Int. Conf. on Coastal Engineering,* Venice, Italy, American Society of Civil Engineers, 474–487.
Masuda, A., Y.-Y. Kuo, and H. Mitsuyasu, 1979: On the dispersion relation of random gravity waves. Part 1. Theoretical framework. *J. Fluid Mech.,* **92,** 717–730.
Mitsuyasu, H., Y.-Y. Kuo, and A. Masuda, 1979: On the dispersion relation of random gravity waves. Part 2. An experiment. *J. Fluid Mech.,* **92,** 731–749.
Norheim, C. A., T. H. C. Herbers, and S. Elgar, 1998: Nonlinear evolution of surface wave spectra on a beach. *J. Phys. Oceanogr.,* **28,** 1534–1551.
Peregrine, D. H., 1967: Long waves on a beach. *J. Fluid Mech.,* **27,** 815–827.
Phillips, O. M., 1960: On the dynamics of unsteady gravity waves of finite amplitude. Part 1. The elementary interactions. *J. Fluid Mech.,* **9,** 193–217.
Schäffer, H. A., P. A. Madsen, and R. Deigaard, 1993: A Boussinesq model for waves breaking in shallow water. *Coastal Eng.,* **20,** 185–202.
Stive, M. J. F., 1984: Energy dissipation in waves breaking on gentle slopes. *Coastal Eng.,* **8,** 99–127.
Thornton, E. B., and R. T. Guza, 1982: Energy saturation and phase speeds measured on a natural beach. *J. Geophys. Res.,* **87,** 9499–9508.
——, J. S. Galvin, F. L. Bub, and D. P. Richardson, 1976: Kinematics of breaking waves. *Proc. 15th Int. Conf. on Coastal Engineering,* Honolulu, HI, American Society of Civil Engineers, 461–476.
Wei, G., J. T. Kirby, S. T. Grilli, and R. Subramanya, 1995: A fully nonlinear Boussinesq model for surface waves. Part 1. Highly nonlinear unsteady waves. *J. Fluid Mech.,* **294,** 71–92.
Whitham, G. B., 1974: *Linear and Nonlinear Waves.* Wiley Interscience, 636 pp.
Willebrand, J., 1975: Energy transport in a nonlinear and inhomogeneous random gravity wave field. *J. Fluid Mech.,* **70,** 113–126.